SOURCE PROCESS OF THE 2003 PUERTO PLATA EARTHQUAKE USING TELESEISMIC DATA AND STRONG GROUND MOTION SIMULATION

Fabricio Moquete Everth* **Supervisor: Yuji YAGI ****
MEE11604 **Toshiaki YOKOI *****

Abstract

Using teleseismic data, the spatial and temporal slip distribution of the 2003 Puerto Plata earthquake in the Dominican Republic, with the recent method, was determined. We obtained the slip distribution over the fault plane, with the following source parameters: (strike, dip and rake) = (110.0º, 8.0º and 76.6 º); seismic moment of M_0 = 1.446×10^{19} Nm (M_w6.7), source duration = 14 sec. These results obtained from the inversion analysis were used as parameters for simulating strong ground motion in the Puerto Plata area and other cities by empirical attenuation formulas for Peak Ground Acceleration (PGA) and Peak Ground Velocity (PGV) with the shortest distance to the coseismic rupture and its moment magnitude. The fault area was estimated to be 30 km x 27 km = 810km^2 from the aftershock distribution obtained by a local seismic network. These PGA and PGV values are converted to the modified Mercalli intensity by using the empirical formula. The obtained values are quite consistent with an isoseismal map with the registered intensity that was felt during the Puerto Plata earthquake.

Keywords: Inversion, Puerto Plata Earthquake, Source Process, Strong Ground Motion.

1. INTRODUCTION

On September 22nd, 2003, at 00:45 (4:45 UTC) the northern part of the Dominican Republic on the Hispaniola Island was severely shaken by an M_w6.5 (NEIC-IRIS) earthquake (Figure 1). A very wide damage was caused on buildings in the major cities of Puerto Plata and Santiago along with landslides in outer areas followed by a large aftershock of M_w5.6 (USGS) about an hour after the main shock. The seismic activity in the aftershock zone increased that year; only in the month of September 208 earthquakes were registered. Also aftershocks ranging up to nearly M_w5.0 continued for over a month, alarming local inhabitants.. The focal mechanism of the main shock and the aftershock zone, along with geological evidence for an active fold-thrust belt offshore of Hispaniola Island, suggests that the earthquake occurred beneath Puerto Plata, on the south dipping thrust fault located offshore (Dolan and Bowman, 2004).

Figure 1. Focal mechanism of the 2003 Puerto Plata earthquake and its largest aftershock, showing the location of the city of Puerto Plata and the two main cities of the country, the Capital city of Santo Domingo and the second most important Santiago de los Caballeros (Global CMT Catalog Search, 2003).

* Seismological Institute of Universidad Autonoma de Santo Domingo.
** Assoc. Professor, Graduate School of Life and Environmental Sciences, University of Tsukuba, Japan.
*** Chief Research Scientist, International Institute of Seismology and Earthquake Engineering, BRI, Japan.

2. METHOD

Yagi and Fukahata (2011) proposed an improved method in which the uncertainty of the Green's Function is included in the inversion analysis. This new method considers the modeling error of the Green's function as shown below.

2.1. Observation equation

In general the observed seismic waveform for the far-field term at a station *j* due to shear dislocation source on a fault plane *S* is given as follows:

$$u_j(t) = \sum_{q=1}^{2} \int_S G_{qj}^0(t,\xi) * \dot{D}_{qj}^0(t,\xi) \mathrm{d}\xi + e_{bj} \qquad (1)$$

For Green's function calculation, P, pP and sP phases are considered together with the receiver response function and inelastic attenuation adding the possibility for the mechanism of those sub-events to change (Figure2).

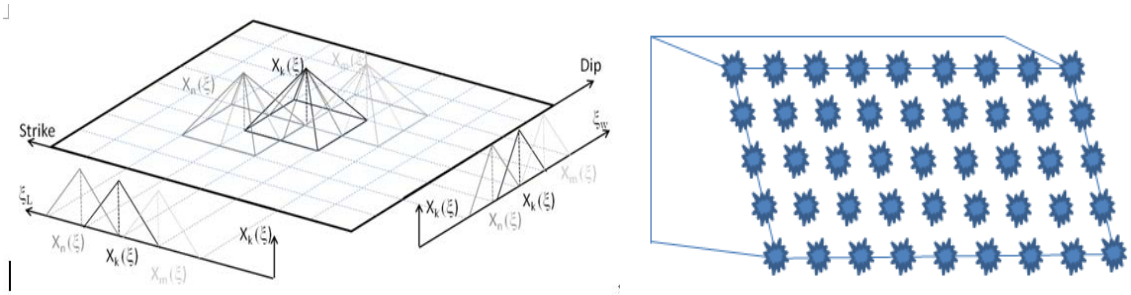

Figure 2. *Left:* Spatial basis function $X_k(\xi)$. *Right:* Finite fault model with multiple point sources of sub-events distributed on the fault plane.

The amplitude and timing of reflection phases in heterogeneous media are the most difficult part in the estimation of the Green's function. The modeling error δg_{qkj} of the Green's function is introduced as:

$$g_{qkj}^0(t) = g_{qkj}(t) + \delta g_{qkj}(t), \qquad (2)$$

This error adds a new term to the observation error e_{bj} as follows:

$$\mathbf{e}_j(\mathbf{a}) = \sum_{q=1}^{2} \sum_{k=1}^{K} \mathbf{P}_{qkj}(\mathbf{a}) \delta \mathbf{g}_{qkj} + \mathbf{B}_j \mathbf{e}_{bj} \qquad (3)$$

2.1.1. Prior Constraints

we use smoothness of slip rate in space and time as prior constraints.

$$\nabla^2 \dot{D}(t,\xi) + e_s = 0; \quad \frac{\partial^2}{\partial t^t} \dot{D}(t,\xi) + e_t = 0, \qquad (4)$$

where the errors e_s and e_t are Gaussian with zero and covariance $\rho_1^2\mathbf{I}$ and $\rho_2^2\mathbf{I}$, respectively.

2.1.2. Akaike's Bayesian Information Criterion

The Akaike's Bayesian Information Criterion (ABIC, Akaike, 1980) expression for a given initial model parameter vector $\mathbf{a}^i$ is as follows:

$$(\alpha^2,\gamma^2) = N log\, s(\mathbf{a}^*) - log\alpha^2|\mathbf{G}_1 + x^2\mathbf{G}_2| + log\left|\mathbf{H}^t\mathbf{C}_d^{-1}(\gamma^2,\mathbf{a}^i)\mathbf{H} + \alpha^2(\mathbf{G}_1 + x^2\mathbf{G}_2)\right| + \log\left|\mathrm{G_d}(\gamma^2,\mathrm{a^i})\right| + \mathrm{C}' \quad (5)$$

Here we used:

$$\sigma_g^2 = s(\mathbf{a}^*)/N, \quad (6)$$

which is derived from the necessary condition that the partial derivative of the ABIC respecting σ_g^2 should be zero.

To reconstruct the spatio-temporal slip-rate distribution $\dot{D}_q$ is the interpolation using a finite number of basis functions (Figure 2 *Left*):

$$\dot{D}_q^0(t,\xi) \cong \sum_{k=1}^{K}\sum_{l=1}^{L} a_{qkl}\, X_k(\xi) T_l(t - t_k) \quad (7)$$

3. DATA

Teleseismic body-wave data was retrieved from the Incorporated Research Institutions for Seismology (IRIS) (http://www.iris.edu/dms/wilber.htm); the following seismic networks were selected:

- ✧ Global Telemetered Seismograph Network (USAF/USGS).
- ✧ Global Seismographic Network (GSN) stations and arrays (IRIS/USGS - IRIS/IDA**)**.

The BHZ channels of more than 16 stations were downloaded and their quality, (e. g. the signal to noise ratio) was checked. The number of stations chosen was 11 (Table 1 and Figure 3) and only P-wave was picked for the analysis and only the stations with epicentral distance between 30 and 90 degrees from the event's location were selected.

Table 1. List of the 11 chosen stations.

No	Stations	Latitude	Longitude	Network
1	AMNO	34.95	-106.46	GSN - IU
2	RSSD	44.12	-104.04	GSN - IU
3	TUC	32.31	-110.78	GSN - IU
4	FFC	54.73	-101.98	GSN - II
5	CPUP	-26.33	-57.33	GTN
6	TRQA	-38.06	-61.98	GSN - IU
7	PLCA	-40.73	-70.55	GTN
8	COLA	64.87	-147.86	GSN - IU
9	BFO	48.33	8.33	GSN - II
10	ANTO	39.87	32.79	GSN - IU
11	TIXI	71.63	128.87	GSN - II

Figure 3. Location of the chosen stations on the planet and the earthquake's epicenter location.

4. INVERSION ANALYSIS

We adopted the epicenter (19.85N 70.67W) and depth (10 km) from the USGS catalog, with a fault mechanism parameters: strike, dip, rake = (110.0º, 10.0º, 85º) from the Global CMT catalog, with magnitude M_w6.5 from NEIC - IRIS as an input parameter for the inversion process.

The minimum ABIC in the tested data was obtained with the depth value of 10 km. Figure 4b shows the graphic with the ABIC values obtained when the dip angle was changed from 8 to 11 degrees at a fixed depth of 10 km. With the dip of 8 degrees the ABIC becomes minimum. For this reason it was decided that the depth should remain 10 km and the dip 8º (Figure 4, a) and b)).

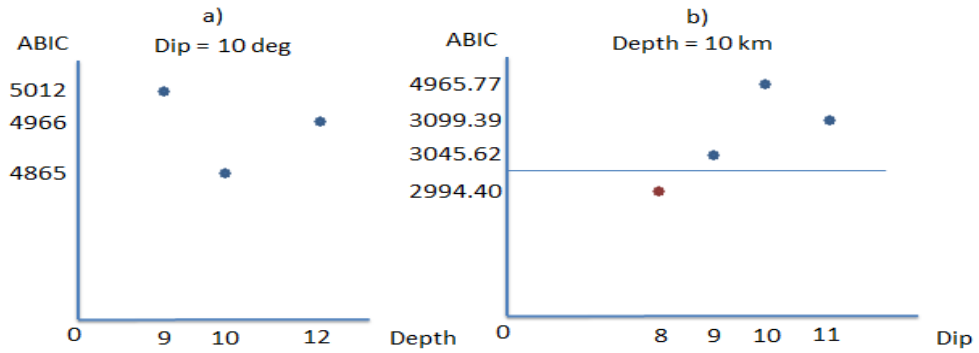

Figure 4. a) ABIC variation with different depth values. b) ABIC variation with different dip angle values; the red dot represents the minimum ABIC obtained.

5. RESULTS AND DISCUSSION

In the inversion method, the fault plane can be identified along with the calculation of the moment magnitude, the dimensions of the fault, the source time function, and a detailed temporal and spatial distribution of slip on the fault.

The time window duration for the Green's function was 50 seconds. There is a series of 15 triangle functions for the slip rate function of every sub-fault with a rise time window of 5 seconds each.

5.1. Inversion Process Outcome

The results are shown in Figure 4. The focal mechanism shows the fault geometry with a rupture duration of 14 seconds and total seismic moment of $M_0 = 1.446\times10^{19}$ Nm (M_w6.7) (Figure 5 *Left*). This seismic moment is higher than the one calculated by the NEIC-USGS ($M_0 = 7.1\times10^{18}$ Nm) (M_w6.5) and the Global CMT ($M_0 = 5.25\times10^{18}$ Nm) (M_w6.4).

In Figure 5 (*left and center*) we can see that the coseismic slip extension along the strike zone coincides with the aftershock distribution of approximately 30 km along the strike zone by which the size of the fault can be roughly estimated.

Figure 5 (*Right)* shows the waveform obtained from the inversion process. The black waveform represents the observed data while the red waveform represents the synthetic waveform from the inversion output. As it is shown in the image, the synthetic and observed waveform matches.

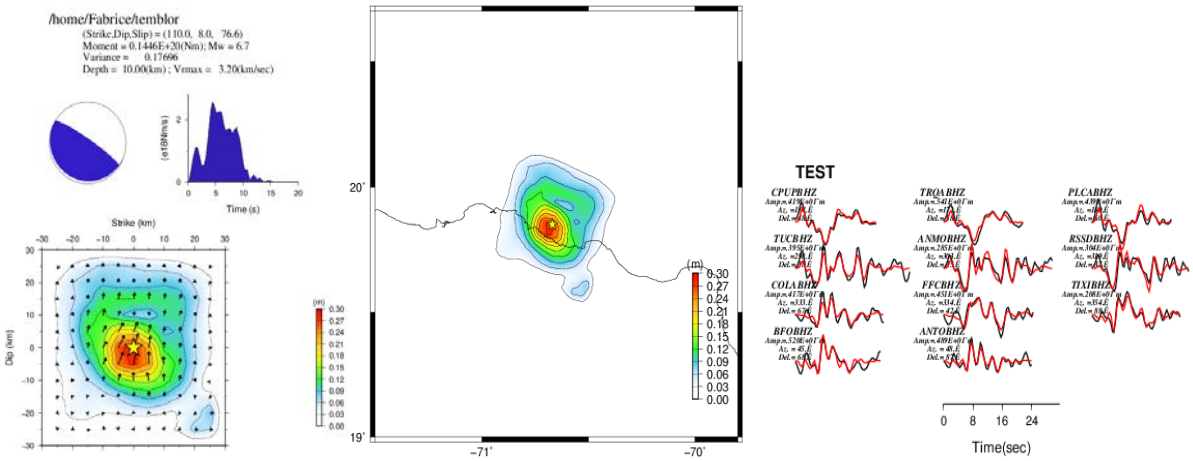

Figure 5. *Left:* Focal mechanism, Source time function and Coseismic slip vectors distribution of the 2003 Puerto Plata earthquake. *Center:* Coseismic slip distribution shown on the map of the Puerto Plata area. *Right:* Comparison between the observed (black) and the synthetic (red) waveform data obtained with the new formulation.

From the results of the inversion it can be seen that the slip amount is higher in the area that surrounds the hypocenter (seismogenic zone) with a maximum slip of 0.30 m (red area) and 0.21 m (yellow area). The red and yellow areas shown in Figure 5 (*left*) are considered as the asperities; the rupture starting point (hypocenter) is almost at the center of this asperity associated with maximum slip. It can be seen that the slip amount in the shallower part ranges from 0.6 m to 0.18 m.

5.2. Strong ground motion simulation

Two different methods were applied in order to simulate the strong ground motion of the Puerto Plata earthquake:

- ✧ Empirical attenuation-distance curves for PGA (peak ground acceleration) and PGV (peak ground velocity): Here the required source information is solely limited to the seismic magnitude and fault area, as types of outer faults parameters.
- ✧ Stochastic Green's Function Method (SGFM): This method simulates the strong ground motion of a large seismic event using synthetic ground motion records of a relatively small event that shares the same source location with that large one in place of the real records in the Empirical Green's Function Method (Irikura and Miyake 2011-2012).

5.2.1 Empirical attenuation relations

The obtained PGA and PGV values, with both methods, when converted to Modified Mercalli Intensity (I_{MM}), using the relationship between PGA, PGV and I_{MM} (Wald et al, 1999) are very close to the values shown in the isoseismal map (Table 3). The calculation was done for latitude and longitude range: (18.0N 20.0N and 68.5W 71.5W). Also, we conducted the same strong motion simulation method to the Latitude and Longitude of the cities of Puerto Plata, Santiago de los Caballeros and the capital city of Santo Domingo using the same parameters mentioned above, and the obtained PGA and PGV values when converted to I_{MM} are also very close to the values registered in the isoseismal map.

Table 3. PGA, PGV and I_{MM} values obtained with the empirical-attenuation curve.

City	Lat.	Lon.	Rupture. Distance (km)	PGA[1]	PGA[2]	PGV[2]	I_{MM}[3]	Obs. I_{MM}
Santo Domingo	18.500	-69.983	146	17.6	18.3	1.0	I-II	IV
Santiago de los C.	19.472	-70.688	29	170.6	175.0	8.2	VI-VII	VII
Puerto Plata	19.800	-70.683	11	341.4	372.2	19.2	VIII	VIII

Note: [1] Fukushima and Tanaka (1990), [2] Si and Midorikawa (1999), [3] Average of the Modified Mercalli Intensity calculated from an average of both PGA values using Wald et al. (1999) and the observed Modified Mercalli Intensity.

5.2.2 Stochastic Green's Function Method

Stochastic Green's Function is calculated using the way of Ohnishi and Horike (2004), and used in place of the real records, afterwards, in the Empirical Green's Function Method.

The synthetic accelerogram and velocity seismograms calculated for the area of Puerto Plata. The PGA and PGV averaged over two horizontal components are 295 cm/s^2 and 15 cm/s. The Fourier spectra of the ground acceleration and pseudo-velocity response are shown in Figure 6; this figure shows an intensity of 5.2 in the JMA scale, which converted to the Mercalli scale is 7.6, this value is quite close to the intensity felt on the Puerto Plata area in the isoseismal map.

Since specific geological data of the ground in the Puerto Plata area was not available, a velocity structure for firm ground (AVS30=300m/s) was assumed, so that the results of the simulation would be closer to real

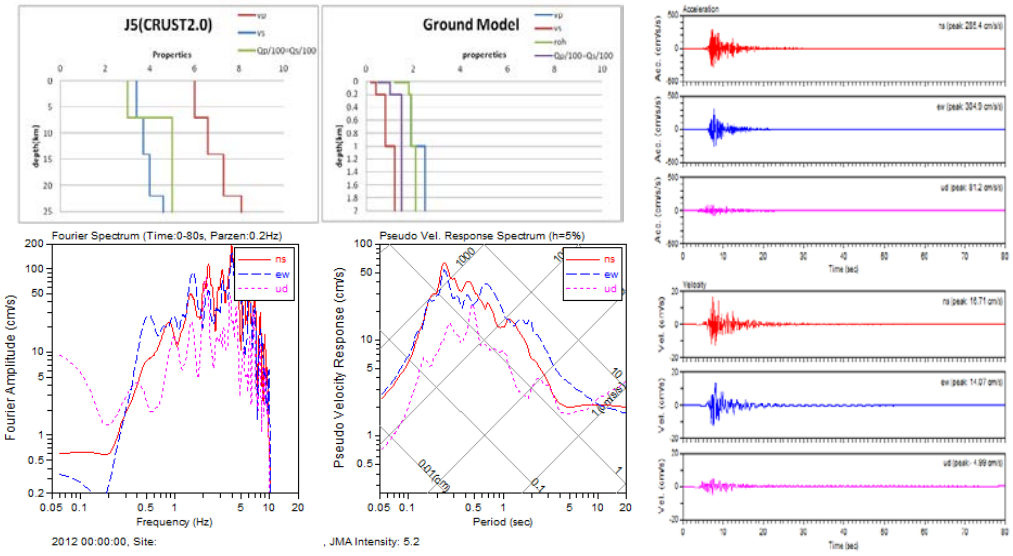

Figure 6. Up: Crustal structure (Type J5 of CRUST2.0, *top-left*). Ground structure used for simulation (*top-center*). Down: Fourier amplitude spectrum of ground acceleration (*bottom-left*) and Pseudo velocity response (*bottom-center*) of the Puerto Plata earthquake: Synthetic strong motion waveform data for acceleration (*top-right*) and velocity.

6. CONCLUSSION

A rupture duration of 14 seconds and total seismic moment of $M_0 = 1.446\times10^{19}$ Nm (M_w6.7). This seismic moment is higher than the one calculated by the NEIC-USGS ($M_0 = 7.1\times10^{18}$ Nm) (M_w6.5) and the Global CMT ($M_0 = 5.25\times10^{18}$ Nm) (M_w6.4), taking around 10 iterations in order to obtain an acceptably small value of ABIC. The slip amount is higher in the area that surrounds the hypocenter (seismogenic zone) with a maximum slip of 0.30 m. This slip distribution along strike matches the fault size estimated on the aftershocks distribution.

With the empirical attenuation curve we can see that the area of the epicenter where the PGA values are within 350 and 400 for both methods and the PGV between 20 and 25; these values converted to I_{MM} are very close to the I_{MM} value near the epicenter in the isoseismal map which is in between 8 and 9. Despite the Stochastic Green's Function Method preciseness, this simulation outcome is not very reliable due to the lack of important data.

7. REFERENCES

Dolan, J. F., and Bowman, D. D., 2004, Seismological Research Letters, 75, 587-591.

Fukushima, Y., and Tanaka, T., 1990, Bull. Seism. Soc. Am. **80**, No. 4, 757-783.

Irikura, K., and Miyake, H., 2011-2012, Lecture notes on Strong Motion Seismology, IISEE/BRI.

Kuge, K., 2010-2011, Earthquake Source Process, IISEE/BRI Lecture note.

Si, H., and Midorikawa, S., 1999, J. Struct. Constr. Eng. AIJ, 523, 63–70 (in Japanese with English Abstract).

Website: Global CMT catalog search http://www.globalcmt.org/CMTsearch.html

Website: U. S. Geological Service (USGS). (http://neic.usgs.gov/neis/eq_depot/2003/eq_030922/).

Yagi, Y., and Fukahata, Y., 2011, Geophysics J. Int. **186**, 711-720.